Electronic Supplementary Material (ESI) for New Journal of Chemistry.

Supporting Information

Tracking Photoinduced Charge Separation in a Perfluorinated Zn-Tetraphenylporphyrin Sensitizer

Daniel H. Cruz Neto, Philipp Gotico, Thu-Trang Tran, Caroline Szantai, Zakaria Halime, Marie Sircoglou, Juan Soto, Karine Steenkeste, Daniel Peláez,* Thomas Pino,*, Minh-Huong Ha-Thi*

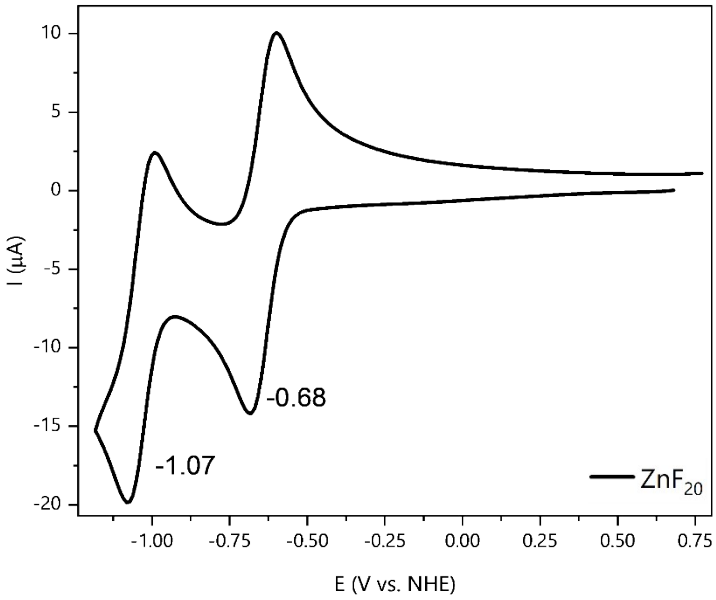

Figure S1. Cyclic voltammogram of 1 mM ZnF_{20} in Ar-saturated CH_3CN (black) and CH_3CN/H_2O (9:1, red), containing 100 mM tertbutylammonium hexafluorophosphate. WE: glassy carbon electode, CE: Pt wire, RE: $Ag/AgNO_3$ (ferrocene was added as internal refe

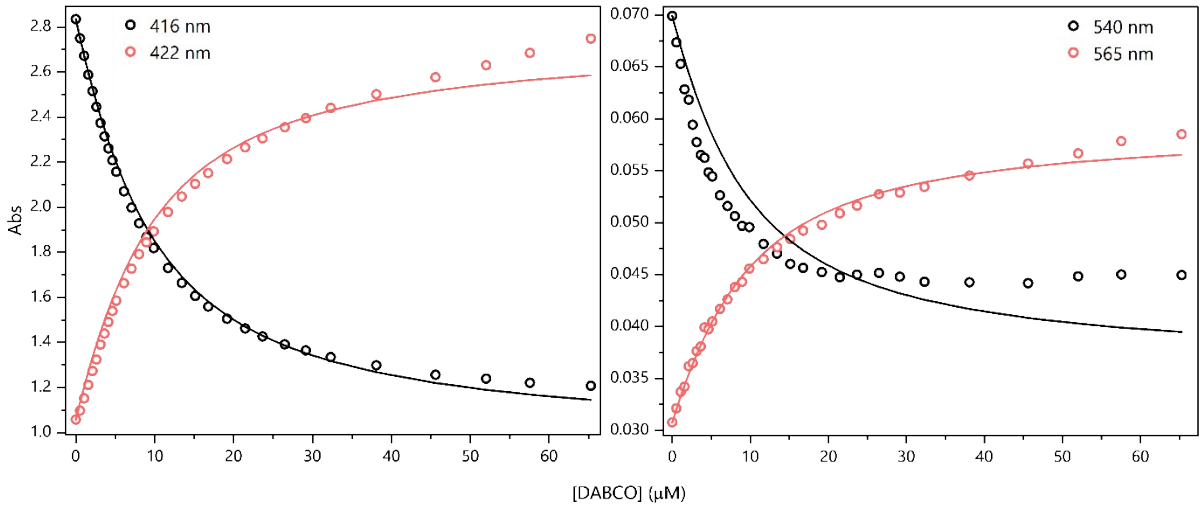

Figure S2. Absorption changes observed on the titration of 4.9 μM ZnF_{20} with DABCO in the Soret region (left) and for the Q-bands (right). Solid lines represent the fit obtained by simulating the system with an ML model, where M = ZnF_{20} and L = DABCO. The corresponding absorption spectra are shown in Figure 2 of the main text. The equilibrium constant β_{11} for the formation of the ML complexe is defined as: $M + L \rightleftharpoons ML$ (β_{11}).

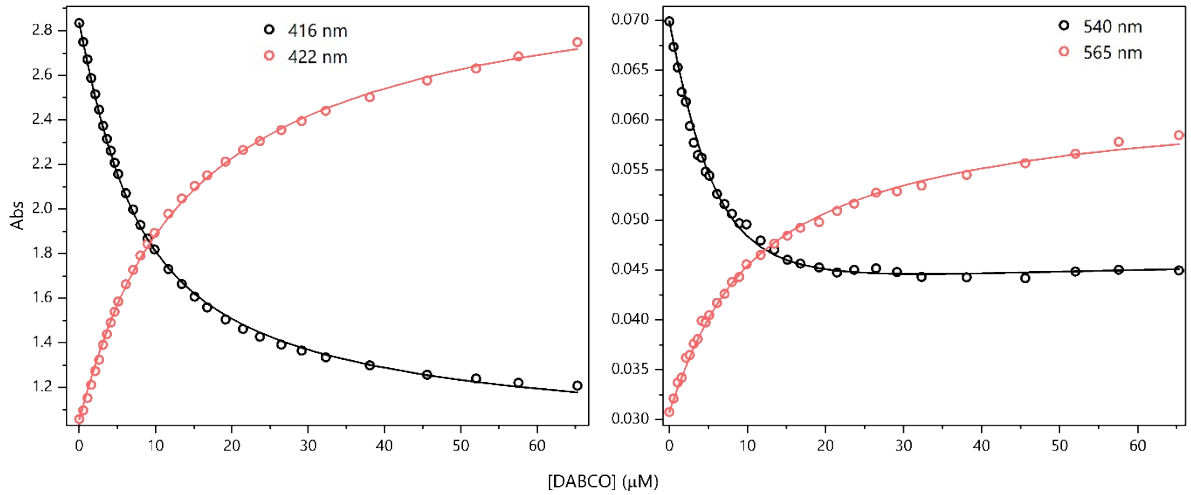

Figure S3. Absorption changes observed on the titration of 4.9 μM ZnF_{20} with DABCO in the Soret region (left) and for the Q-bands (right). Solid lines represent the fit obtained by simulating the system with an ML_2 model, where M = ZnF_{20} and L = DABCO. The corresponding absorption spectra are shown in Figure 2 of the main text. The global equilibrium constants β_{11} and β_{12} for the formation of the ML and ML_2 complexes are defined as: $M + L \rightleftharpoons ML$ (β_{11}), and $M + 2L \rightleftharpoons ML_2$ (β_{12}).

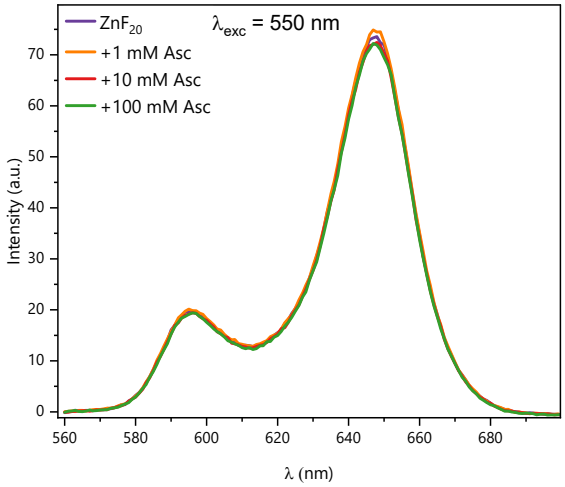

Figure S4. Emission spectra of ZnF_{20} (4.9 μM) upon addition of different concentrations of ascorbate in CH_3CN/H_2O (6:4). λ_{exc} = 550 nm.

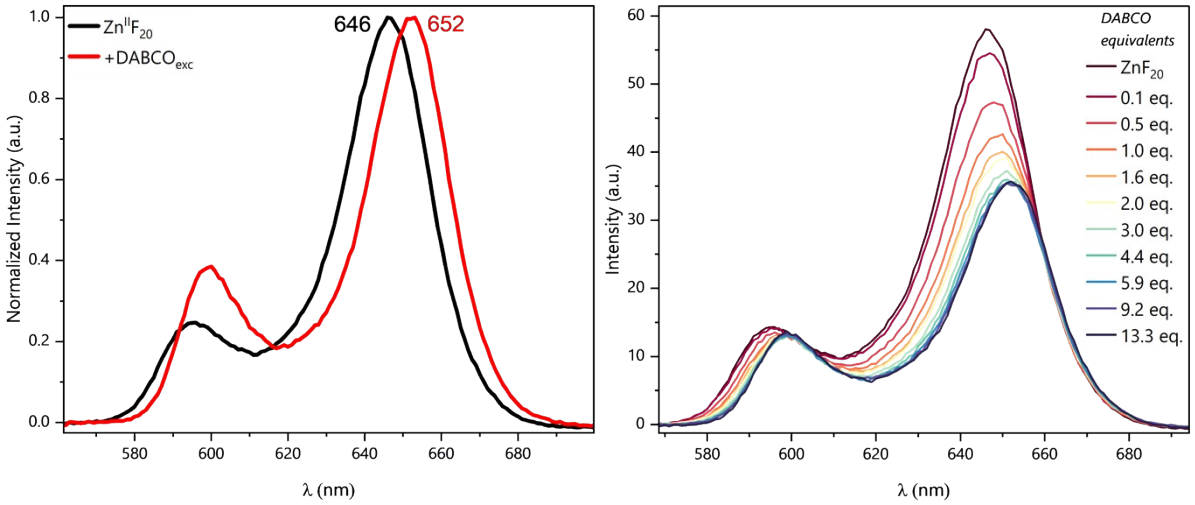

Figure S5. Left panel: normalized emission spectra of 5.4 µM ZnF_{20} alone and in the presence of 100 mM DABCO in CH_3CN. Right panel: steady state emission spectra of 5.4 µM ZnF_{20} upon titration with DABCO, showing emission quenching in the presence of the coordinating donor. λ_{exc} = 550 nm.

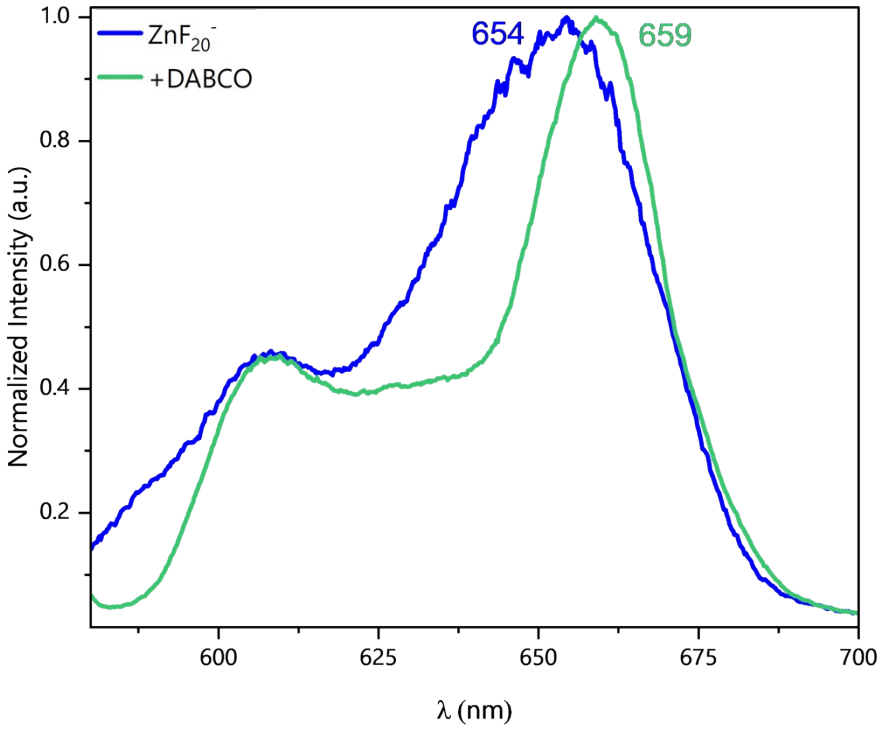

Figure S6. Normalized emission spectra of chemically-reduced ZnF_{20} alone (blue, λ_{exc} = 555 nm) and in the presence of 100 mM DABCO (green, λ_{exc} = 565 nm) in CH_3CN. Chemical reduction was achieved upon addition of 1 eq. $CoCp_2$ as a reducing agent.

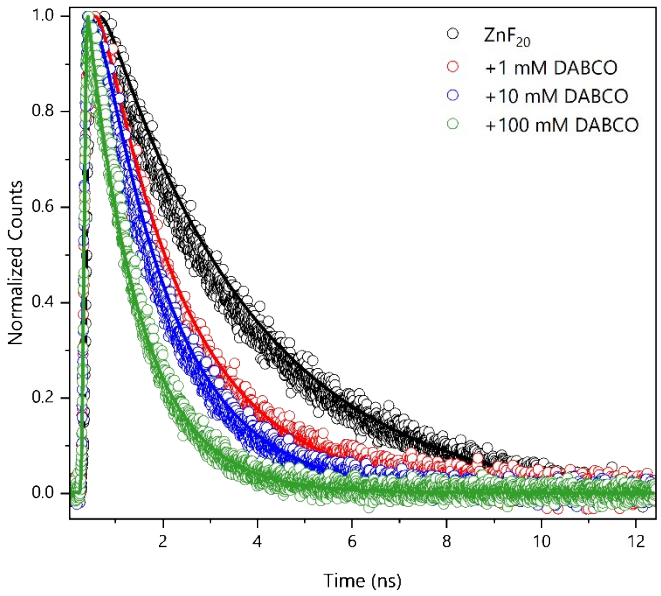

Figure S7. Fluorescence decay of ZnF_{20} in the presence of different concentrations of DABCO in CH_3CN. Two photon excitations at 800 nm.

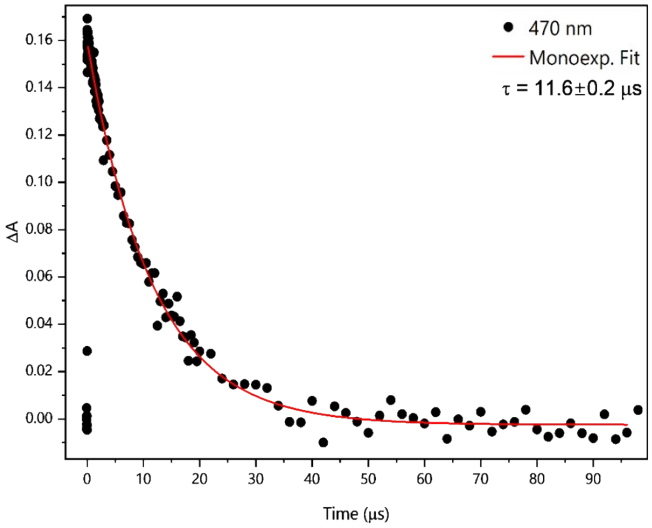

Figure S8. Kinetic decay recorded at 470 nm of 5.8 µM ZnF_{20} in CH_3CN with the corresponding monoexponential fit generating a time constant of τ = 11.6 ± 0.2 µs. OTA spectra are shown in Figure 3a of the main text. λ_{exc} = 423 nm, 1 mJ/pulse.

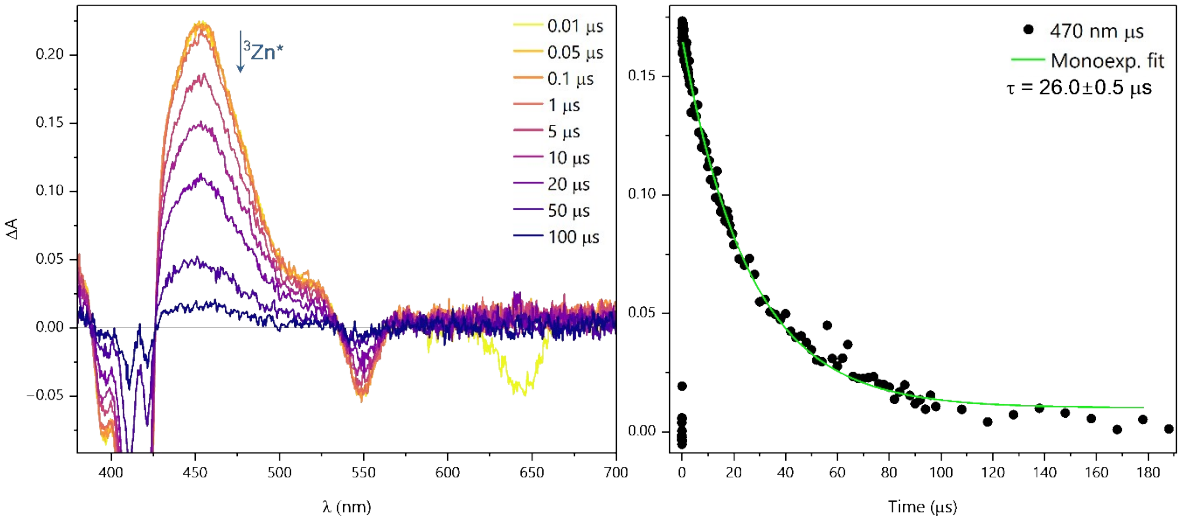

Figure S9. Transient absorption spectra (left panel) of 5.8 µM ZnF_{20} in CH_3CN/H_2O (6:4) and the corresponding monoexponential fit generating a time constant of τ = 26 ± 0.5 µs (right panel). λ_{exc} = 423 nm, 1 mJ/pulse.

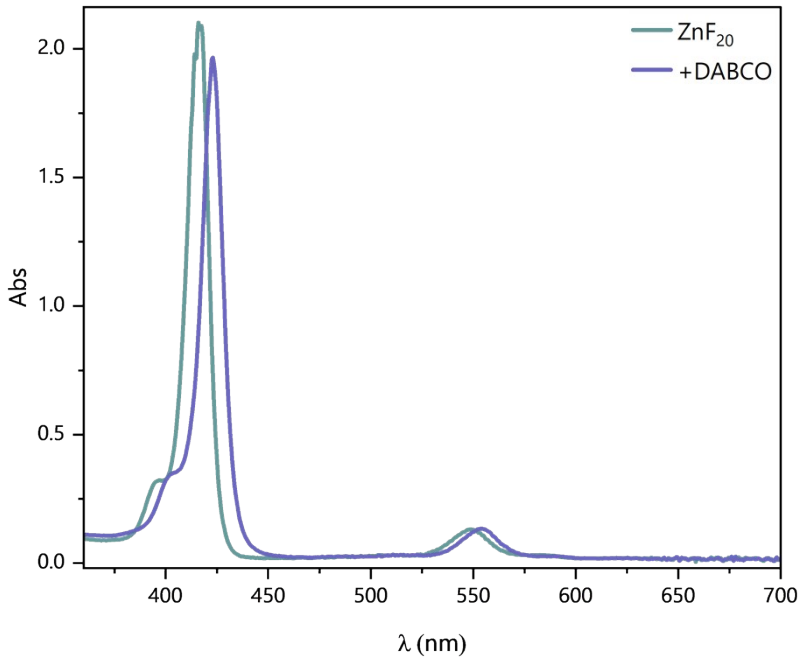

Figure S10. Absorption spectrum of the sample containing 5.8 µM ZnF_{20} (green) and upon addition of 100 mM DABCO (purple).

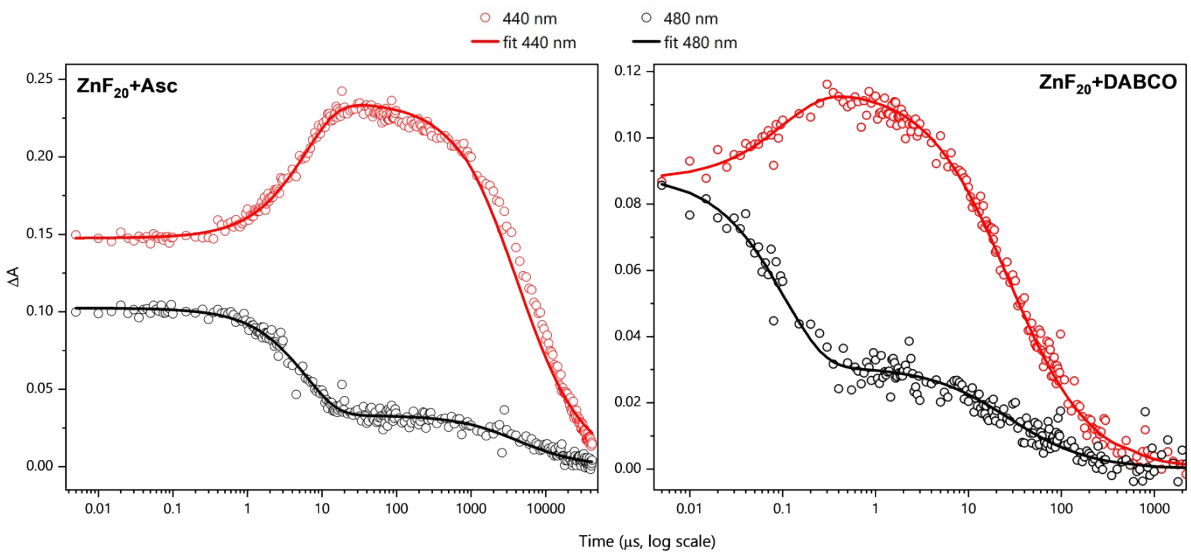

Figure S11. Fitting at selected wavelengths from the spectro-kinetic simulations obtained with the bimolecular reactions presented in Table S1 for (left) ascorbate. For DABCO, biexponential functions were used to fit the dataset (right). The corresponding transient spectra are presented in Figure 3.

Table S1. Bimolecular reaction model used for the simulation of spectro-kinetic data and the corresponding rate constants. ED = electron donor.

#	Reaction	ED = DABCO	ED = Asc
k_q	$^3Zn^* + ED \rightarrow Zn^I + ED^+$	1.3 (± 0.1) ×10^7 s^{-1}	1.5 (± 0.5) ×10^6 $M^{-1}s^{-1}$
k_{rec}	$Zn^I + ED^+ \rightarrow Zn + ED$	2.6 (± 0.8) ×10^{10} $M^{-1}s^{-1}$	1.3 (± 0.4) x10^8 $M^{-1}s^{-1}$

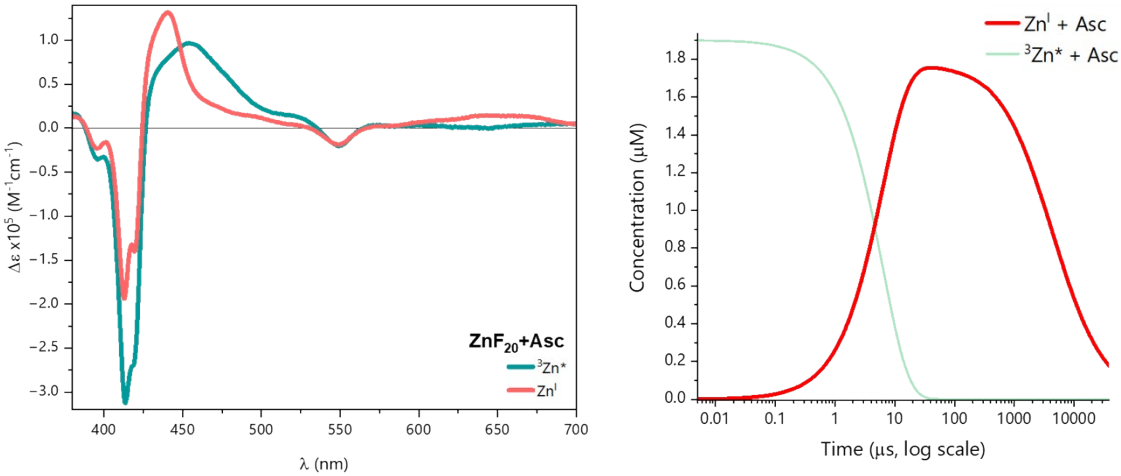

Figure S12. Species-associated difference spectra (SADS) obtained from the spetro-kinetic simulations performed with the bimolecular reactions presented in Table S1 the ascorbate-containing system (left). The corresponding evolution of the transient species is shown on the right panel.

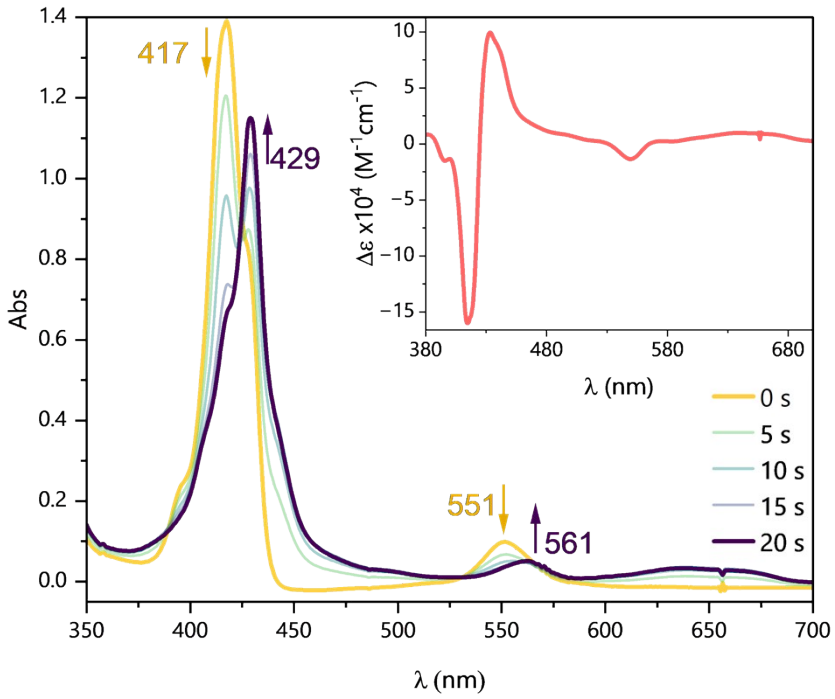

Figure S13. Photoaccumulation measurements on 4.8 µM ZnF_{20} using 1 mM BIH as a sacrificial electron donor in CH_3CN. Inset: differential spectrum. λ_{exc} = 405 nm, 58 mW.

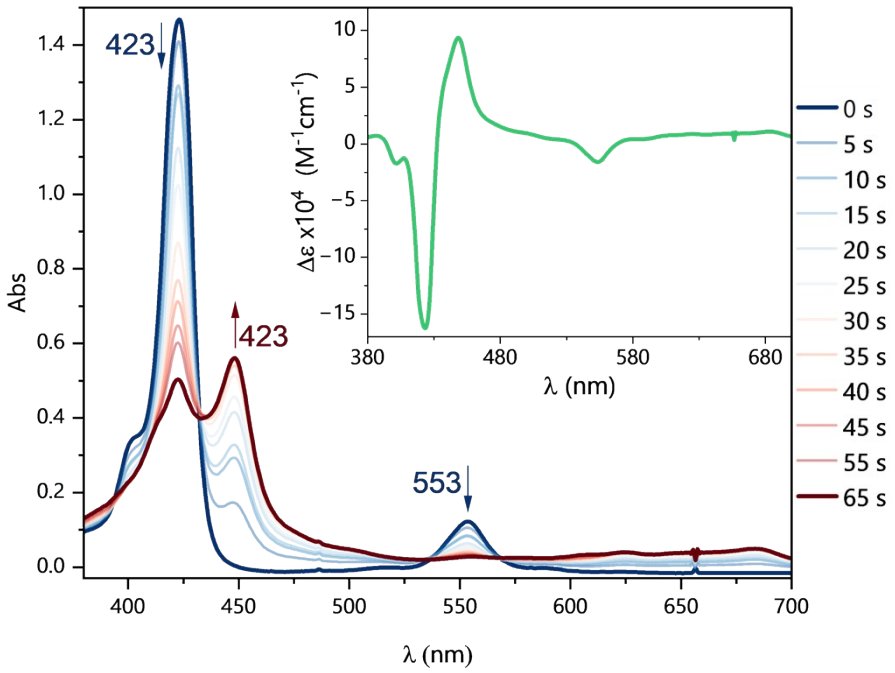

Figure S14. Photoaccumulation measurements on 4.8 µM ZnF_{20} in the presence of 5 mM DABCO and using 1 mM BIH as a sacrificial electron donor in CH_3CN. Inset: differential spectrum. λ_{exc} = 405 nm, 58 mW.

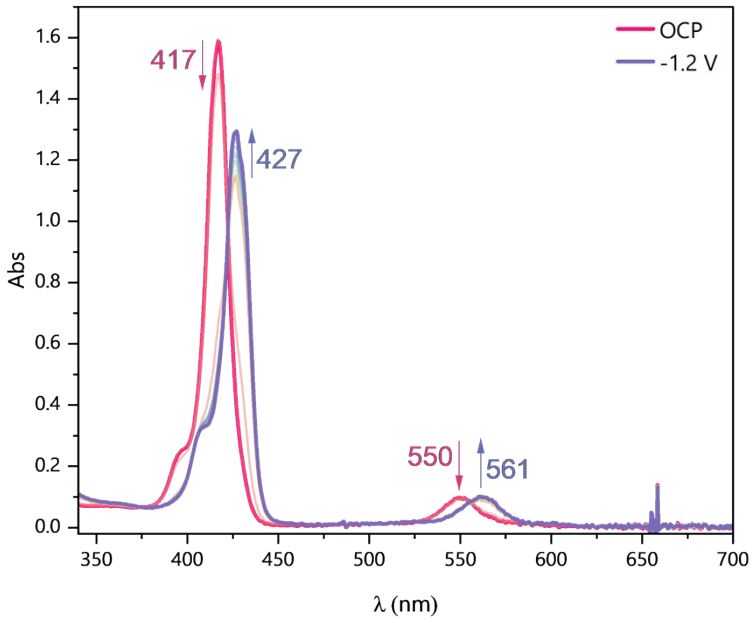

Figure S15. UV-Vis spectroelectrochemical experiments with ~45 µM ZnF_{20} in the presence of 100 mM $TBAPF_6$ in deaerated CH_3CN before (pink) and after (violet) applying -1.2 V vs. Ag/Ag^+ on a Pt-mesh working electrode.

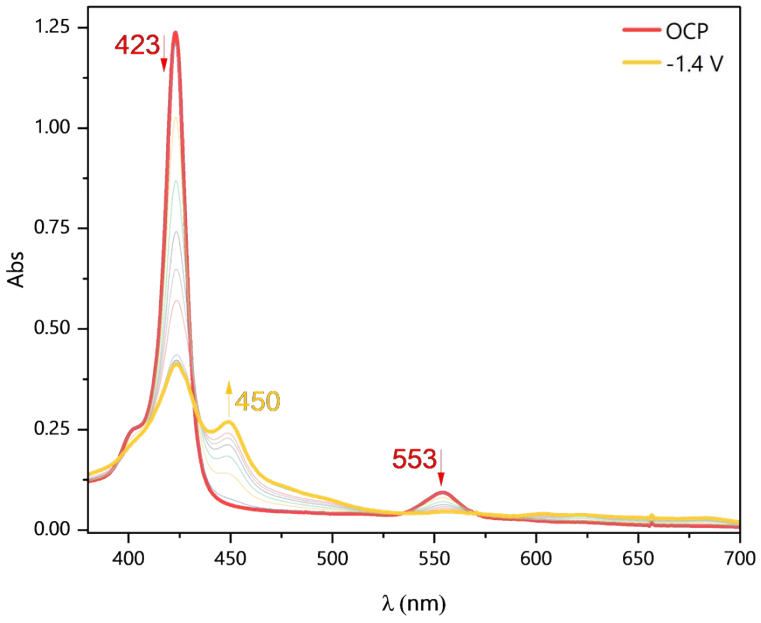

Figure S16. UV-Vis spectroelectrochemical experiments with ~45 µM ZnF_{20} in the presence of 100 mM DABCO and 100 mM $TBAPF_6$ in deaerated CH_3CN before (red) and after (yellow) applying -1.4 V vs. Ag/Ag^+ on a Pt-mesh working electrode.

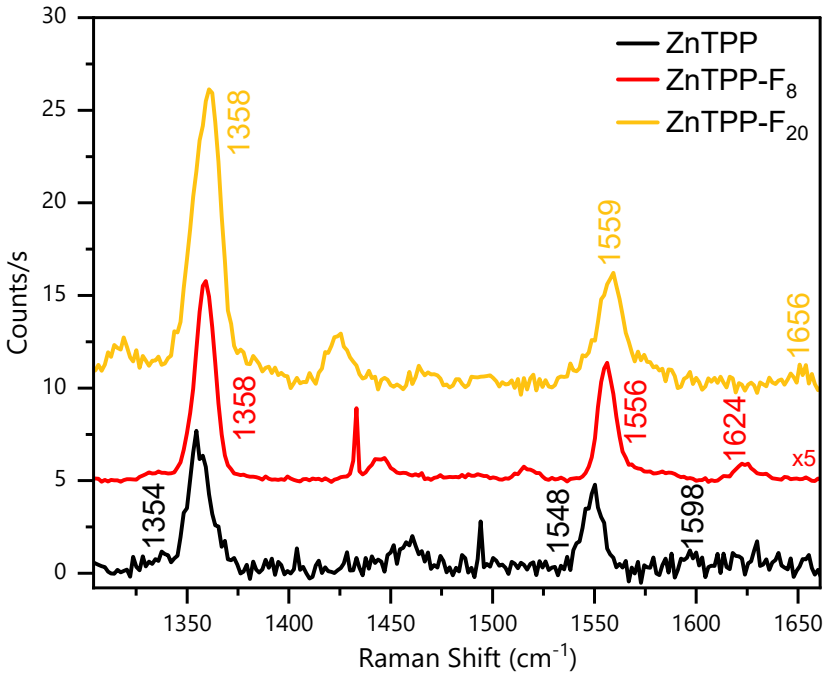

Figure S17. Resonance Raman spectra of ZnTPP, ZnTPP-F_8, and ZnTPP-F_{20} showing the effect of the fluorine atoms on the observed normal modes of the porphyrin. The effect of fluorine substitution on the phenyl rings is clearly shown on the bands with a strong phenyl character – 1656 cm^{-1}, for instance. Spectra were recorded in solid state with λ_{exc} = 405 nm, 30 mW.

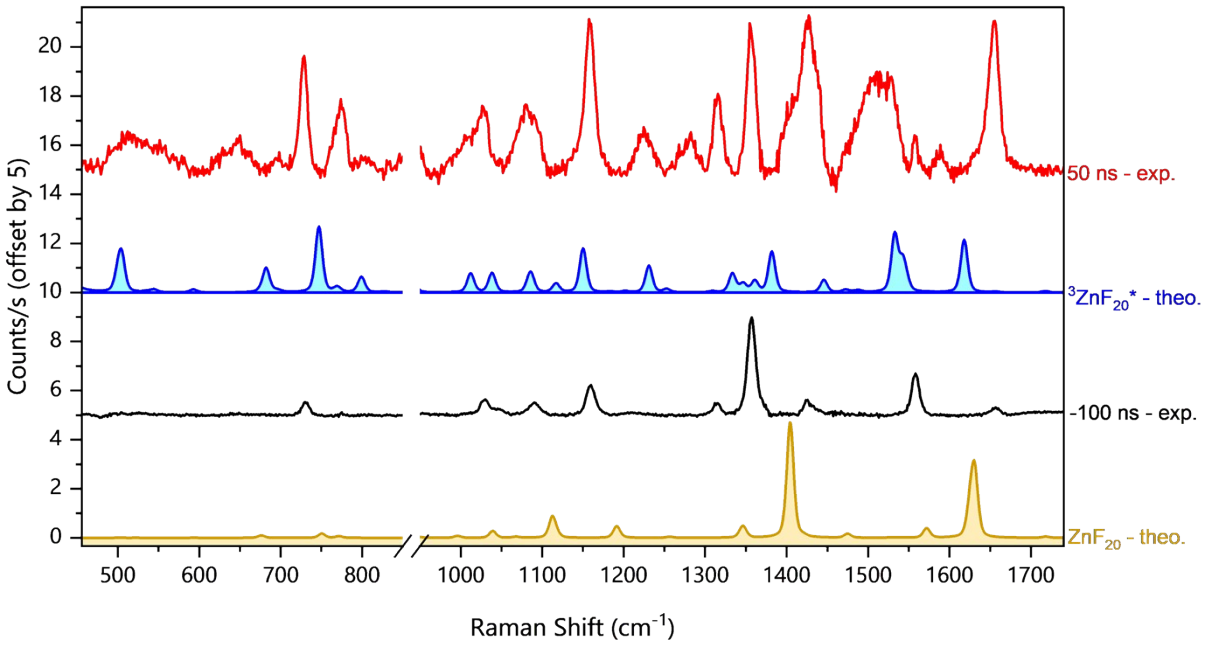

Figure S18. Comparison between theoretical and experimental resonance Raman spectra. Experimental spectra at -100 ns and 50 ns were obtained with 12.6 µM ZnF_{20} in CH_3CN – raw dataset in Figure 4 of the main text. The theoretical spectra were simulated for ZnF_{20} in the ground state, and for the T1 state of the porphyrin. It is worth mentioning that the experimentally recorded triplet state (at 50 ns) contains contributions of the ZnF_{20} in the ground state.

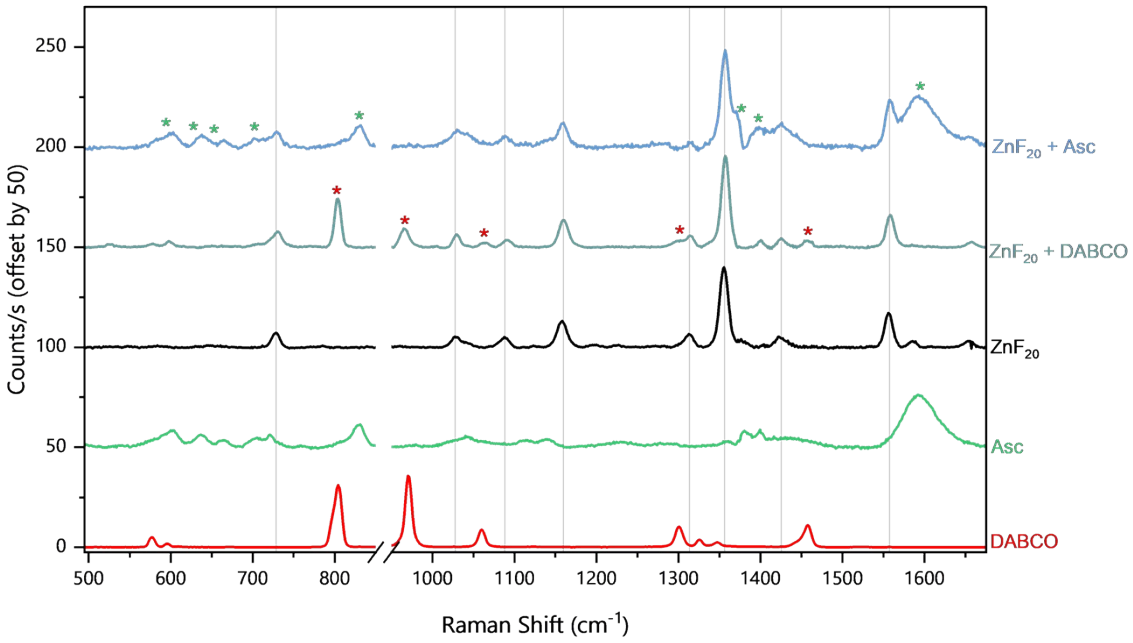

Figure S19. Comparison between the experimental spectra of 12.6 µM ZnF_{20} alone (black) and in the presence of 100 mM DABCO (pale green) and 100 mM Asc (pale blue). The reference spectra of 100 mM DABCO (red) and 100 mM ascorbate (green) alone are added for comparison. Red asterisks represent the vibrational modes of DABCO, and green asterisks represent the vibrational modes of ascorbate. Solid vertical black lines are markers of the vibrational modes of ZnF_{20}. λ_{pump} = 554 nm, 2.2 mJ/pulse; λ_{probe} = 447 nm, 2.2 mJ/pulse.

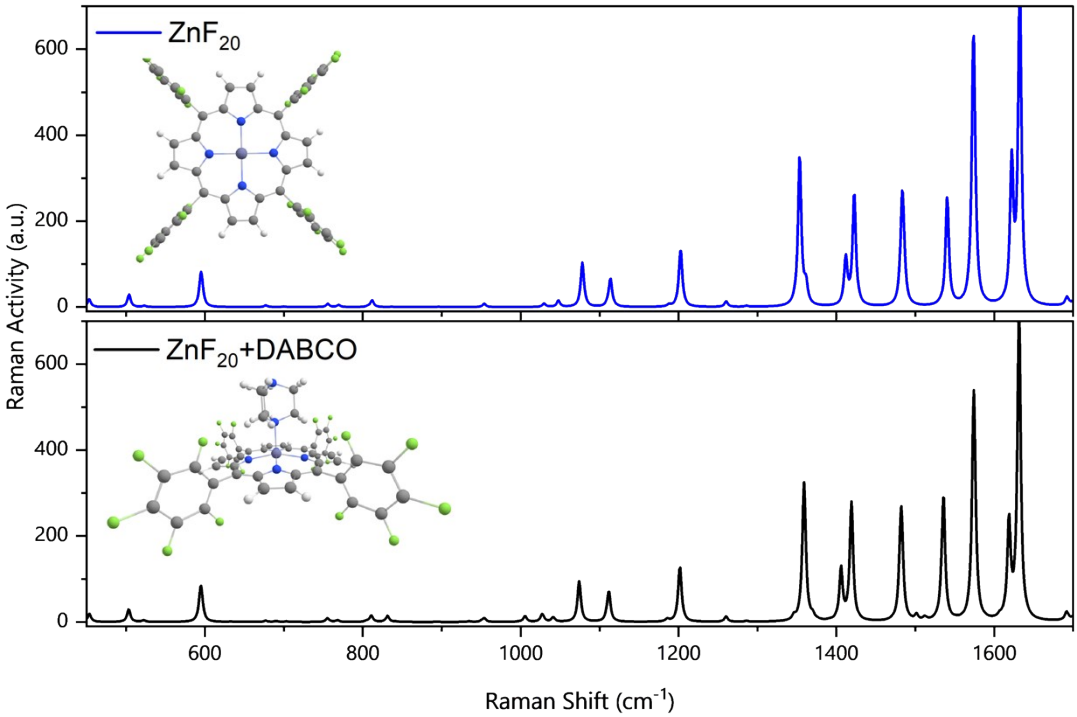

Figure S20. Non-resonant theoretical spectra for ZnF_{20} (top panel) and for the ZnF_{20}-DABCO 1:1 complex (bottom panel). The presence of DABCO coordinated to the porphyrin center does not affect the vibrational modes of the ZnF_{20}.

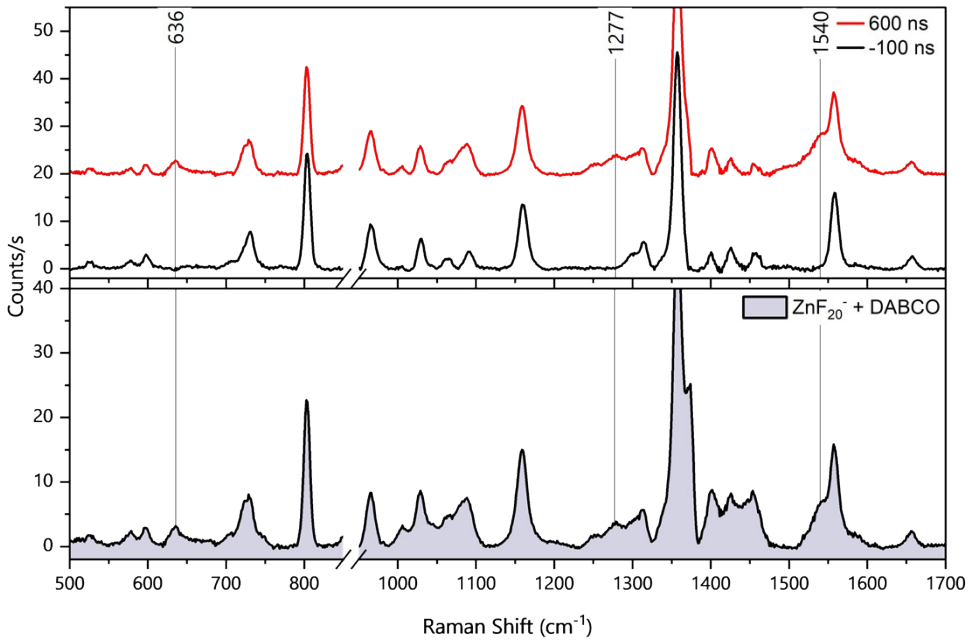

Figure S21. Comparison between the experimental TR3 spectra of 12.6 µM ZnF_{20} in the presence of 100 mM DABCO the reference reduced state obtained by chemical reduction. Top panel: TR3 spectra at -100 and 600 ns; bottom panel: spectrum of ZnF_{20}^{-} chemically produced by the addition of 1 eq. $CoCp_2$ in the presence of 100 mM DABCO. Solid lines mark the bands observed for the reduced state.

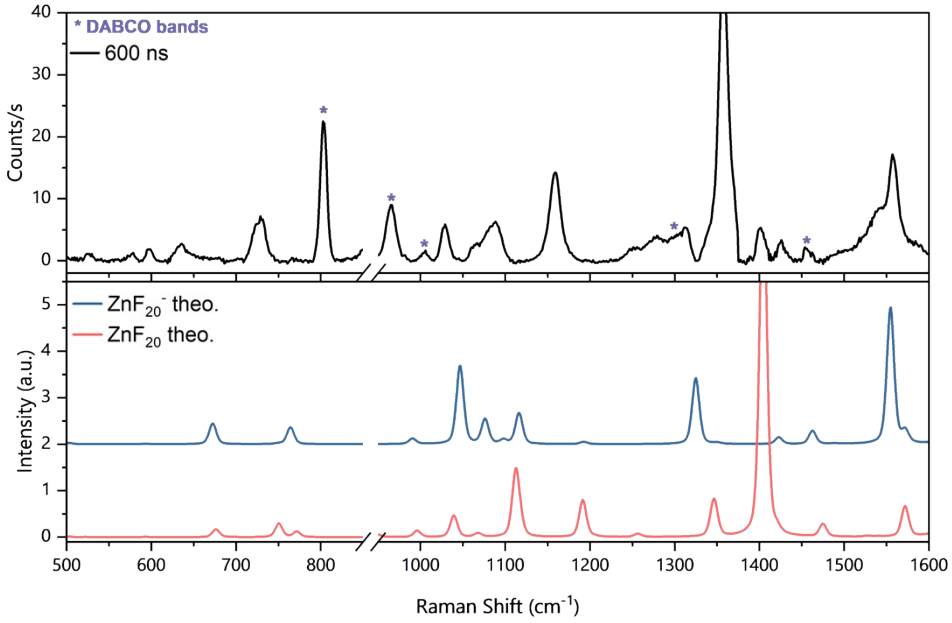

Figure S22. Top panel: TR3 spectrum of 12.6 µM ZnF_{20} in the presence of 100 mM DABCO at 600 ns delay, which corresponds to the maximal signature of ZnF_{20}^{-}-$DABCO^{+}$; normal modes of DABCO are marked with an asterisk. Bottom panel: non-shifted theoretical spectra, in resonance conditions, obtained for ZnF_{20} in the ground state (red) and ZnF_{20}^{-} (blue).

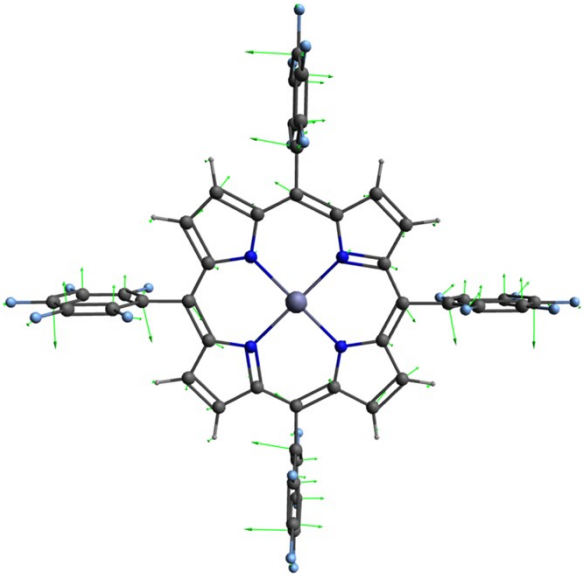

Figure S23. Vibrational mode detected for Zn^{I}-$DABCO^{+}$ at 636 cm^{-1} (experimental) tentatively assigned to an out-of-plane phenyl vibration [π_3', γ(CF)] calculated at 672 cm^{-1} (theoretical). Green arrows are representative of the non-normalized force constants.

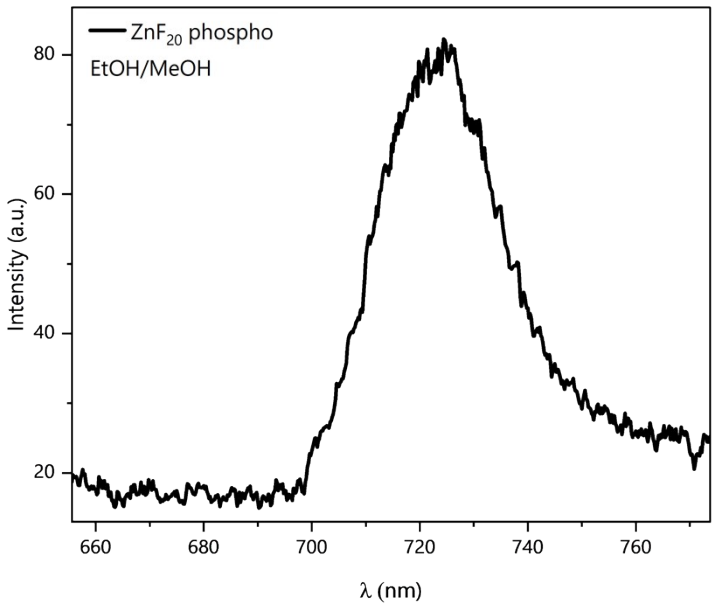

Figure S24. Phosphorescence spectrum of ZnF_{20} recorded in an ethanol/methanol (EtOH/MeOH) mixture at 77 K. λ_{exc} = 555 nm.